Measurement of quadrupolar coupling constants, shielding tensor elements and the relative orientation of quadrupolar and shielding tensor principal axis systems for rubidium-87 and...

ARTICLE *in* THE JOURNAL OF PHYSICAL CHEMISTRY · JANUARY 1990

Impact Factor: 2.78 · DOI: 10.1021/j100365a014

3 AUTHORS, INCLUDING:

John C Edwards
Independent Researcher
74 PUBLICATIONS **915** CITATIONS

SEE PROFILE

Measurement of Quadrupolar Coupling Constants, Shielding Tensor Elements, and the Relative Orientation of Quadrupolar and Shielding Tensor Principal Axis Systems for Rubidium-87 and Rubidium-85 Nuclei in Rubidium Salts by Solid-State Nuclear Magnetic Resonance

John T. Cheng, John C. Edwards, and Paul D. Ellis*

Department of Chemistry, University of South Carolina, Columbia, South Carolina 29208
(Received: April 4, 1989)

The spin lattice relaxation time, T_1, quadrupolar coupling constant, Q_{cc}, and chemical shielding tensor elements of several rubidium salts have been surveyed at the frequency 130.88 MHz for ^{87}Rb and 38.64 MHz for ^{85}Rb, i.e. 9.4T, or 400 MHz for ^{1}H's. Typical relaxation times for ^{87}Rb are in the range of 100–300 ms and 50–300 ms for ^{85}Rb. The Q_{cc} values are in the range of 7–14 MHz for ^{85}Rb and 3–11 MHz for ^{87}Rb. A program was created to numerically simulate and fit experimental powder patterns for the $\pm^1/_2$ central transition, where the principal axis systems (PAS) of the shielding and quadrupole tensors are not coincident. The analysis shows that having both nuclides available with significantly different quadrupole coupling constants makes the general line-shape problem more tractable. That is, the ^{85}Rb data provides an excellent visualization of chemically different rubidium atoms when there are significant differences in the value of Q_{cc}. Such data would be difficult to extract from the corresponding ^{87}Rb line shapes due to the smaller value of Q_{cc}. The ^{87}Rb nuclide, however, because of its smaller value of Q_{cc}, provides an excellent opportunity to observe the consequences of the noncoincident PAS frames between the shielding and quadrupole tensors.

Introduction

Rubidium has two stable isotopes, ^{85}Rb ($I = {}^5/_2$) and ^{87}Rb ($I = {}^3/_2$), which are amenable to the NMR experiment. The natural abundances of these nuclides are 72.8% and 27.2% for ^{85}Rb and ^{87}Rb, respectively. Typically, only the $\pm^1/_2$ central transition is observed in solid-state rubidium NMR. The other transitions are very broad, and the quadrupole coupling constant is sufficiently large to prevent excitation of these transitions. The moderate sensitivity (0.0478 for ^{87}Rb, 0.007 for ^{85}Rb relative to ^{1}H's) and efficient relaxation (100–300 ms for pure salts, ~1 ms for the surface adsorbed species) make rubidium nuclei a potentially favorable probe for study in the solid state via NMR methods.

Alkali-metal salts serve as promoters in several heterogeneously catalyzed industrial reactions, e.g. the partial oxidation of ethylene to ethylene oxide[1,2] and the partial oxidation of *o*-xylene to phthalic anhydride.[3] A detailed knowledge of the nature of the adsorbed species present in such catalytic systems can only help to understand the mechanism(s) of this promotion. Cheng and Ellis[4] have utilized the ^{87}Rb nucleus as a probe to explore the nature of cation adsorption and dynamics on γ-alumina. The results of that work suggest this approach is promising as a means to explore surface structure. Further, their approach will be employed to study other surfaces such as transition aluminas, α-alumina, clays, and zeolites.

The work summarized here can be divided into two parts. The first portion is a survey of the central transitions of several rubidium compounds. These compounds include rubidium halides and rubidium nitrate, which give rise to narrow resonances because of the small value of the quadrupolar coupling constant, and rubidium chromate, acetate, sulfate, and hydroxide, which give rise to reasonably wide resonances. The resulting quadrupole coupling constants, chemical shifts, relaxation times, and the various line shapes were used as important benchmarks for the study of the adsorption of ^{87}Rb$^+$ on the γ-alumina surfaces and will continue to be used in future studies of other surfaces. Likewise, these data should prove helpful in the understanding of the temperature dependency of the NMR line shape and how such changes reflect structural transitions in the solid state.

The second portion deals with the development of an *interactive graphical curve fitting* (IGCF) program and its application to the problem of the disentanglement of the relative orientation of the principal axis system frames of a pair of second rank tensors, namely the quadrupole and anisotropic shielding tensors. Here we will outline the development of a seven-parameter (Q_{cc}, δ_Q, δ_{cs}, η_{cs}, α, β, γ) variable size simplex algorithm approach to the analysis of these line shapes. A graphics oriented program written in the C language has been designed to handle the general curve fitting on either a PC-AT or MicroVax by either manual or auto searching. To perform its task the program utilizes a nonlinear regression analysis for the various types of line shapes.

Experimental Methods

Chemical Analysis and NMR Measurements. Rubidium salts were purchased from Alfa Products, Morton Thiokol, Inc., and were used without further purification. Single crystals can be grown readily from bulk salts such as Rb_2SO_4, $RbNO_3$, and Rb_2CrO_4 at room temperature without special treatment. The NMR line shapes of powders ground from these pure crystals are identical with those of the original samples taken directly from the bottle. Rubidium hydroxide, purchased from the GFS Company, was found through simple titration experiments to contain one water of hydration. Hence, this compound should be referred to as $RbOH{\cdot}H_2O$.

The NMR measurements were made on a Varian XL-400 spectrometer operating in the so-called "wide-line" mode. The resonance frequency for ^{87}Rb on this spectrometer is 130.88 MHz and 38.64 MHz for ^{85}Rb. The spectra were obtained by using a broad-band, tunable Doty Powder Probe from Doty Scientific (Columbia, SC). All chemical shifts, expressed as either parts per million or kilohertz, are reported with respect to 1.0 M $RbNO_3$ solution. The *nonselective* $\pi/2$ pulse width was determined from a liquid sample of $RbNO_3$, typical values being in the range of 7–8 μs. The selective solid echo pulse sequence described previously[4] was employed for the selective observation of the central $\pm^1/_2$ transition of the rubidium nuclei.

Theory

Baugher et al.[5] have extensively discussed the line shape of the central transition ($\pm^1/_2$) for a quadrupolar nucleus. To simplify

(1) Brengle, A. S.; Sobrante, E.; Stewart, H. R. U.S. Patent 2,709,173. Sacken, D. K. U.S. Patent 2,671,764. Nielson, R. P. U.S. Patent 3,702,259. Nielson, R. P.; LaRochelle, J. H. U.S. Patent 3,962,136; 4,356,312; 4,010,115; 4,012,425.

(2) Kanoh, H.; Nishimura, T.; Ayame, A. *J. Catal.* **1979**, *57*, 372.

(3) Wachs, I. E.; Chan, S. S.; Saleh, R. Y. *J. Catal.* **1985**, *91*, 366. Wachs, I. E. U.S. Patent 4,582,912.

(4) Cheng, J. T.; Ellis, P. D. *J. Phys. Chem.* **1989**, *93*, 2549.

(5) Baugher, J. F.; Taylor, P. C.; Oja, T.; Bray, P. J. *J. Chem. Phys.* **1969**, *11*, 4914.

0022-3654/90/2094-0553$02.50/0

his analysis, he assumed the principal axis system (PAS) of the anisotropic shielding tensor and quadrupole tensor to be coincident. Such an assumption leads to a significant reduction in the complexity of the analysis, but yields a line shape that in many cases does not correspond to the experimental data. The resonance frequency of the central transition is dependent on the orientation of the PAS of the quadrupole tensor relative to the magnetic field $\mathbf{H}_0$, the orientation of the PAS of the anisotropic shielding tensor relative to the magnetic field, and the relative orientation of the two tensors with respect to each other. To illustrate his approach we will outline his calculation.

In the presence of an anisotropic shielding interaction the chemical shift Hamiltonian can be expressed as follows:

$$h_{CS}(\theta,\phi) = \omega_0[(\sigma_{11}) \sin^2\theta \sin^2\phi + (\sigma_{22}) \sin^2\theta \cos^2\phi + (\sigma_{33}) \cos^2\theta]I_z \quad (1)$$

where σ_{11}, σ_{22}, and σ_{33} are the three principal values of the chemical shielding tensor, ω_0 is the resonance frequency of nucleus, and ϕ, θ are Euler angles relating the magnetic field $\mathbf{H}_0$ to the PAS of the chemical shielding tensor of the nucleus. We can also express eq 1 in the form

$$h_{CS}(\theta,\phi) = \omega_0[\sigma_0 + (\delta/2)\{(3\cos^2\theta - 1) - \eta \sin^2\theta \cos 2\phi\}]I_z \quad (2)$$

where

$$\sigma_0 = \tfrac{1}{3}(\sigma_{11} + \sigma_{22} + \sigma_{33}) \qquad \delta = \sigma_{33} - \sigma_0$$

$$\eta = \sigma_{22} - \sigma_{11}/\delta \qquad \sigma_{33} \geq \sigma_{22} \geq \sigma_{11}$$

In the presence of a quadrupolar interaction the quadrupolar Hamiltonian can be expressed by eq 3.

$$h_{\pm 1/2}(\theta,\phi) = -(R/6\omega_0)[A(\phi) \cos^4\theta + B(\phi) \cos^2\theta + C(\phi)] \quad (3)$$

where

$$R = \omega_q^2[I(I+1) - 3/4]$$

$$A(\phi) = (-27/8) - (9/4)\eta \cos 2\phi - (3/8)\eta^2 \cos^2 2\phi$$

$$B(\phi) = (30/8) - (\eta^2/2) + 2\eta \cos 2\phi + (3/4)\eta^2 \cos^2 2\phi$$

$$C(\phi) = (-3/8) + (\eta^2/3) + (\eta/4) \cos 2\phi - (3/8)\eta^2 \cos^2 2\phi$$

$$\omega_q = 3e^2qQ/2I(2I-1)\hbar = 3Q_{cc}/2I(2I-1)\hbar$$

$$\eta = (V_{11} - V_{22})/V_{33} \qquad q = (1/e)V_{33}$$

V_{11}, V_{22}, and V_{33} are the values of the three principal elements of the electric field gradient tensor, Q is the quadrupole moment, and ϕ and θ are the same Euler angles described in the chemical shift interaction.

The total Hamiltonian expressed by Baugher et al. is simply the addition of eq 2 and 3 to give the following:

$$H = h_{CS} + h_{\pm 1/2} \quad (4)$$

For a more general case, one has to consider the second rank tensor properties of both the quadrupole and shielding tensors. One cannot simply add two tensor quantities without considering the relative orientation of one tensor with respect to the other. In this case, there is no reason to believe that the PAS for the anisotropic shielding tensor will be coincident with that of the quadrupole tensor. Hence, the first step in the analysis of a problem of this type is to place the tensors in a common reference frame. As the quadrupole interaction is the more dominant interaction, it is convenient to express the shielding tensor in the frame of the quadrupole tensor. Thus, the quadrupolar resonance frequency is considered the same as that in eq 3. To obtain the Hamiltonian of the anisotropic chemical shielding tensor in this frame, we will utilize the standard method of employing Wigner rotation matrices. In the rotating frame, the secular chemical shift Hamiltonian can be expressed as

$$H_{CS} = \omega_0\sigma_0 I_z + \gamma T_{20} R_{20} \quad (5)$$

$$T_{20} = (2/3)^{1/2} I_z B_z$$

To calculate the chemical shielding powder line shape in the presence of the second-order quadrupole effects, the first step is to transform the shielding Hamiltonian from the laboratory frame to the PAS frame of the quadrupole via angles $\Omega = (0, \theta, \phi)$. Then, from the PAS frame of the quadrupole we have to express the shielding tensor in terms of its PAS values. To do this we will carry out a further transformation in terms of the fixed angles (α,β,γ), which relate the quadrupole PAS frame to the shielding PAS frame, i.e.

$$R_{20} = \sum_n D_{0,n}^{(2)}(0, \theta, \phi)^* r_{2n} = \sum_n D_{n,0}^{(2)}(-\phi, -\theta, 0) r_{2n}$$

$$H_{CS} - \omega_0\sigma_0 I_z = \gamma T_{20}[D_{00}(-\phi,-\theta,0)r_{20} + D_{-10}(-\phi,-\theta,0)r_{2-1} + D_{10}(-\phi,-\theta,0)r_{21} + D_{-20}(-\phi,-\theta,0)r_{2-2} + D_{20}(-\phi,-\theta,0)r_{20}] \quad (6)$$

where $D_{n,m}$ are the Wigner rotation matrix[6] elements. When these elements are incorporated into this equation, eq 6 has the following form:

$$H_{CS} - \omega_0\sigma_0 I_z = \gamma T_{20}[((3\cos^2\theta - 1)/2)r_{20} - (3/8)^{1/2} \sin 2\theta e^{-i\phi} r_{2-1} + (3/8)^{1/2} \sin 2\theta e^{i\phi} r_{21} + (3/8)^{1/2} \sin^2\theta e^{-2i\phi} r_{2-2} + (3/8)^{1/2} \sin^2\theta e^{i2\phi} r_{22}] \quad (7)$$

$$T_{20} = (2/3)^{1/2} I_z B_0$$

At this point the shielding tensor is transformed from the quadrupole PAS to its own PAS frame and r_{2m} can be expressed as

$$r_{2m} = \sum_n D_{mn}^{(2)}(\alpha,\beta,\gamma)^* \rho_{2n} = \sum_n D_{nm}^{(2)}(-\gamma,-\beta,-\alpha)\rho_{2n} \quad (8)$$

Further

$$\rho_{20} = (3/2)^{1/2}\delta \quad \text{and} \quad \rho_{2\pm 2} = -(1/2)\eta\delta$$

$$\delta = (2/3)[\sigma_{33} - 1/2(\sigma_{11} + \sigma_{22})]$$

$$\eta = (\sigma_{11} - \sigma_{22})/(\sigma_{33} - \sigma_0)$$

and all other ρ_{2n} are zero. Substitution of all the r_{2m}, D_{nm}, and T_{20} in eq 8 into eq 7 yields eq 9; this gives us the shielding Hamiltonian of the chemical shift, which has been transformed to the quadrupole PAS frame, expressed in terms of its value in the shielding frame:

$$H_{CS} - \omega_0\sigma_0 I_z = (\omega_0 I_z\delta/2)[(3\cos^2\theta - 1)(((3\cos^2\beta - 1)/2) - (\eta/2)\sin^2\beta \cos 2\gamma) + \sin 2\theta \cos(\phi + \alpha)\{-1.5 \sin 2\beta - \eta \sin\beta \cos\beta \cos 2\gamma\} + \sin 2\theta \sin(\phi + \alpha)\{\eta \sin\beta \sin 2\gamma\} + 0.5 \sin^2\theta \cos(\phi + \alpha)\{3\sin^2\beta - \eta \cos 2\gamma(1 + \cos^2\beta)\} + 0.5 \sin^2\theta \sin 2(\phi + \alpha)\{2\eta \cos\beta \sin 2\gamma\}]$$

Note that when $(\alpha, \beta, \gamma) = (0, 0, 0)$ eq 9 reduces to eq 4. In our line-shape simulations the Hamiltonian of the system is the sum of eq 3 and 9 as well as the Zeeman term.

Results and Discussion

A. Relaxation Times. Table I summarizes the spin lattice relaxation time, T_1, data for several ^{85}Rb and ^{87}Rb salts in the solid state. These T_1 values fall into the range 100–300 ms for ^{87}Rb and 50–300 ms for ^{85}Rb. These relatively short values of T_1 make it possible to study the rubidium nucleus at the moderately low concentrations of 10%–2% by weight. An adequate signal to noise ratio can be obtained typically in a few hours since

(6) Mehring, M. *The Principles of High Resolution NMR in Solids*, 2nd ed.; New York Press: 1976.

TABLE I: Spin Lattice Relaxation Time, T_1, of ^{85}Rb and ^{87}Rb in Pure Salts

compd	^{87}Rb, ms	^{85}Rb, ms
pure salt		
$RbClO_4$	224	80
RbOH	180	70
Rb_2CrO_4	200	80
$RbOOCH{\cdot}H_2O$	144	70
$RbOOCCH_3{\cdot}H_2O$	130	40
Rb_2SO_4	210	120
Rb_2CO_3	192	60
$RbNO_3$	100	60
RbF	220	70
RbCl	303	310
RbBr	270	260
RbI	270	270
solution		
1 M $RbNO_3$		2
$RbNO_3$	2.5[a]	
surface salt		
$RbNO_3$	71	
surface species		
$RbNO_3$	0.8	

[a] From ref 8.

the $\pi/2$ pulse employed can excite the spins every second, which is about 5 times T_1.

In Table I, we have also summarized some solution T_1 values for $^{87}Rb^+$ and $^{85}Rb^+$. Typical values are ~2 ms, which is rapid when compared to >10 s for other alkali metals such as $^{133}Cs^+$ and $^7Li^+$. Lindman[7] has extensively discussed the relaxation theory for the alkali-metal ions in solution. The dominant relaxation mechanism is quadrupolar, arising from a time modulation of the electric field gradient (EFG) in the liquid state.

A smaller amplitude is expected for the motional modulation of the EFG for nuclei in a nearly rigid lattice of a salt; consequently the relaxation time of rubidium nuclei for the variety of salts shows much slower relaxation times, on the order of 100 ms. In comparison, ^{133}Cs in $CsNO_3$ has a much smaller Q_{cc} and thus has a much longer relaxation time, on the order of several hours. The quadrupolar mechanism appears to strongly govern the relaxation rate for rubidium nuclei in the solid state. That is, the magnitude of the relaxation times seems to parallel the value of the quadrupole coupling constant. The rubidium halides, which have a small Q_{cc}, have the longest T_1 values in the range of 220–300 ms, compared to the other salts with higher values of Q_{cc} with T_1 values of 100–224 ms. However, the exact correspondence between rubidium and cesium relaxation rates is not clear at the present time. The question as to whether or not there should be a factor of at least 36 000 in the relaxation times of $CsNO_3$ and $RbNO_3$ will be a topic of further research.

Cheng and Ellis[4] have studied the adsorption of $^{87}Rb^+$ on γ-alumina by solid-state NMR. The spectra clearly show the presence of two different types of species: a surface salt and a surface species. With the surface salt, the ion pairs are strongly associated, while with the surface species the ion pairs are well separated. From Table I, the relaxation time of surface salt $RbNO_3$ is quite close to that of the pure salt. The surface species show significantly faster relaxation times of ~0.8 ms, which is even faster than that of Rb^+ in the liquid phase. From relaxation theory, the fastest relaxation rates occur at the T_1 minimum, i.e. when the spectral density for the motion contributes maximally to the relaxation rate. One would expect T_1 values in this region to be between those for rapid motion (small ions in solution) and slow, vibrational motion (rigid lattice ions in a solid). The higher relaxation rate of $^{87}Rb^+$ in the surface species, compared to that of $^{87}Rb^+$ in the liquid, can be explained by the fact that the surface species is undergoing moderate motion on the surface, which, when combined with a potential increase in the Q_{cc} caused by a lowering of the symmetry of the species by absorption to the surface, leads to a shorter relaxation time. The frequency of motion of $^{87}Rb^+$ in the surface species has been estimated to be 10–20 KHz by Cheng and Ellis.[4]

(7) Lindman, B.; Forsen, S. *NMR and the Periodic Table*; Harris, R. K., Mann, B. E., Eds.; Academic Press: New York, 1978.

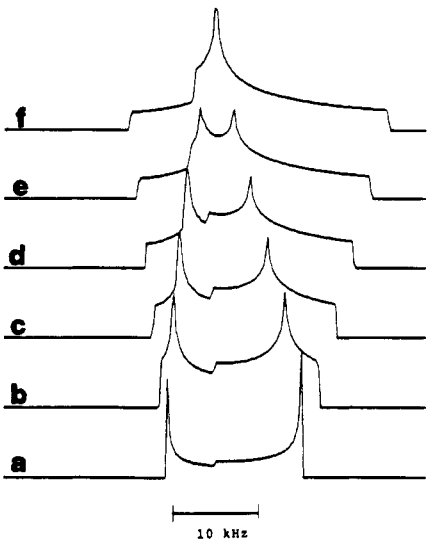

Figure 1. Simulated ^{87}Rb central transition line shapes for a pure second-order quadrupole interaction with Q_{cc} = 4 MHz, $I = {}^3/_2$, and ν_0 = 130.8 MHz, at the following values of η_Q: (a) 0.0, (b) 0.2, (c) 0.4, (d) 0.6, (e) 0.8, (f) 1.0.

B. Extraction of NMR Parameters by Line-Shape Simulation. Unlike pure chemical shift powder line shapes, where the three principal values of the anisotropic shielding tensor can be directly obtained from the line shape almost by inspection, the NMR parameters in the presence of a quadrupolar interaction must be obtained through a detailed line-shape analysis similar to the method of Baugher,[5] but allowing the PAS frames to be noncoincident. This approach is based on solving a given set of nonlinear equations that relate the observed singularities in the observed line shape to the various parameters.

In practice, nonperfect pulses, dipolar broadening, and superposition of chemically different tensors cause the singularities of the line shape to be less sharp or not as distinguishable. Therefore, the measurement of NMR parameters by this method will have some degree of error due to uncertainties in the measurement of a peak or shoulder for a given line shape. To solve this problem, a program is needed to numerically compute the powder pattern line shape for a given set of NMR constants. This theoretical line shape is then compared with the experimental one. Generally, several modifications of the NMR constants are needed until these two line shapes match. Therefore, the calculation will be iterative in nature.

At this point in the analysis we will assume that chemical dynamics are not contributing to the observed line shapes. As a result of this assumption, one can simplify the line-shape program by performing the calculation in the frequency domain. Several techniques[8] that directly calculate the NMR powder pattern in the frequency domain have been reported. Alderman et al.[9] have demonstrated a more efficient method of tiling the unit sphere, which leads to programs that are many times faster than other methods. Instead of producing a histogram by uniformly dividing the spectral width into a large number of bins, this orientation selected technique calculates the intensity for a small segment of the crystal orientation by an interpolation scheme and then transfers the intensity at this frequency to the computed spectra. With this method it only takes about 20 s of MicroVax central processing unit (CPU) time to calculate each theoretical powder

(8) Pake, G. E. *J. Chem. Phys.* **1948**, *168*, 327. Abragam, A. *The Principles of Magnetic Resonance*; Oxford University Press: Oxford, England, 1961; p 216. Pines, A.; Gibby, M. G.; Waugh, J. S. *Chem. Phys. Lett.* **1972**, *15*, 373. Spiess, H. W. *Chem. Phys.* **1974**, *6*, 217. Spiess, H. W.; Grosescu, R.; Haeberlen, U. *Ibid*, **1974**, *6*, 226.

(9) Alderman, D. W.; Solum, M. S.; Grant, D. M. *J. Chem. Phys.* **1986**, *84*, 3717.

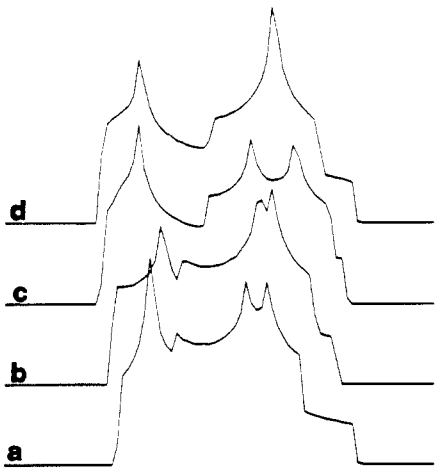

Figure 2. Simulated ^{87}Rb central transition line shapes for noncoincident PAS frames of the quadrupole and CSA tensors. The line shapes are calculated for various sets of Euler angles (α, β, γ), shown in radians, for the situation $I = {}^3/_2$, $\sigma_{11} = -3.0$ kHz, $\sigma_{22} = 0.0$ kHz, $\sigma_{33} = 3.0$ kHz, $Q_{cc} = 4$ MHz, $\eta_Q = 0.3$, and $\nu_0 = 130.88$ MHz. Values of (α, β, γ): (a) (0.5, 1.0, 1.5), (b) (1.0, 1.5, 0.5), (c) (1.5, 0.5, 1.0), (d) (0.5, 0.5, 0.5).

pattern line shape, whereas our old technique, based on summation of the signal in the time domain and subsequent Fourier transform (FT), takes between 2 and 15 min depending upon the angular resolution. A significant fraction of the time difference between frequency domain calculations and those in the time domain is due to the inefficiency of the tiling of the unit sphere in the time domain calculations.

The PAS frames of the anisotropic shielding and quadrupole tensors have been found to be noncoincident in a ^{51}V single-crystal NMR study of V_2O_5 by Gornostansky.[10] It would be rather interesting to check whether the powder line shapes of rubidium salts also reveal this phenomenon. Figure 1 illustrates the numerically computed line shapes for a pure quadrupole interaction under the condition that $Q_{cc} = 4$ MHz, $I = {}^3/_2$, $\nu_0 = 130.88$ MHz, for various η_Q values between 0.0 and 1.0. Note, there can be at most two positions for peaks and four positions for shoulders. On the assumption of coincident frames, the addition of a chemical shielding anisotropy (CSA) interaction will not change the total numbers of peaks and shoulders, but the frequency of a given peak and shoulder will be shifted. Figure 2 summarizes the simulated line shapes for the central transition for noncoincident frames of the anisotropic shielding and quadrupole tensors. The line shapes are calculated for various sets of Euler angles (in radians) (α, β, γ: (0.5, 1.0, 1.5), (1.0, 1.5, 1.0), (1.5, 0.5, 1.0), and (0.5, 0.5, 0.5)) under the condition that $\sigma_{11} = -3$ kHz, $\sigma_{22} = 0$ kHz, $\sigma_{33} = 3$ kHz (the CSA value is set intentionally to meet the real scale of ^{87}Rb), $\eta_Q = 0.3$, $\nu_0 = 130.88$ MHz, and $Q_{cc} = 4$ MHz. Interestingly, this figure shows that there are more than six singularity positions in the simulated line shape and the overall line shape is more complicated than the case where the PAS frames are coincident.

To extract the NMR parameters from a given spectrum by a simulation program is not trivial for the case of noncoincident frames. The Baugher method cannot be applied to solve this problem, but can only provide starting guess data sets for the simulations. There are a total of seven parameters, the η_{CS} and δ_{CS} of the chemical shielding tensor, three Euler angles, Q_{cc}, and η_Q. It would be tedious and time-consuming for a random initial guess to be used on a specific data set for a simulated line shape. We have developed a so-called mother–child (MC) program to resolve this problem. Figure 3 illustrates the basic ideal of this approach. The mother program, such as the IGCF program, does the simplex search, treats the child program (simulation program) as an external function call, and feeds the child program a suitable argument (data input file) containing the NMR parameters. Then it evaluates the difference between the experimental spectrum and

(10) Gornosstansky, S. D.; Stager, C. V. *J. Chem. Phys.* **1968**, *48*, 1416.

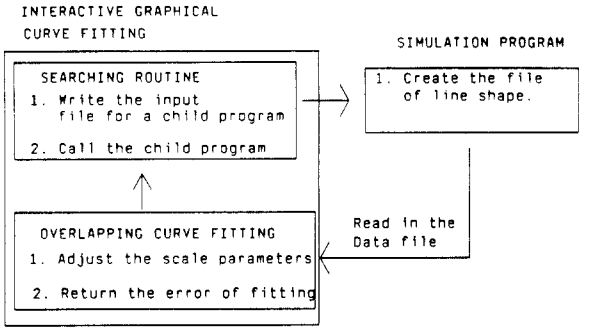

Figure 3. Flow chart of the mother–child program.

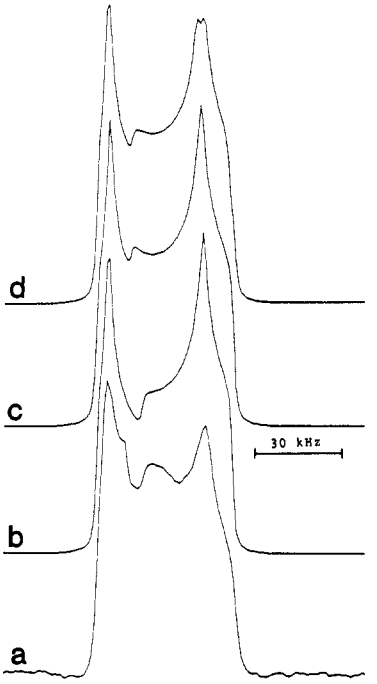

Figure 4. Comparison of experimental and simulated central transition powder pattern line shapes of ^{85}Rb in $RbClO_4$ obtained by two different methods: (a) experimental powder pattern line shape, (b) simulated powder pattern line shape with only the quadrupolar parameters optimized, (c) simulated line shape for a data set obtained by the Baugher method, (d) simulated line shape assuming noncoincident PAS frames obtained by the MC method.

the simulated result. The user is allowed to adjust the width, vertical scale, and displacement of the simulation curve so that some of the NMR parameters, which only affect the width or scale of the line shape, need not be optimized in the simulation. The adjustment can be done manually or autosearched. The index of the difference will then guide the program to find the best data set for the simulation. The advantage of the MC idea is that the simulation program can come from a different source and there is no need to merge that program into the mother program, which at times can be very difficult or impossible.

Figure 4a shows a typical example of an experimental line shape for ^{85}Rb when there is only one type of Rb^+ ion in the unit cell; in this case $RbClO_4$ is the salt. At room temperature $RbClO_4$ has an orthorhombic crystal structure with four molecules per unit cell. The space group is reported to be $F43m$;[12] therefore all Rb^+ sites in the lattice are chemically equivalent. Figure 4b is the simulated ^{85}Rb line shape obtained from a variation of the quadrupole tensor only. Figure 4c is the simulated ^{85}Rb line shape obtained from the Baugher method discussed above; values obtained are $\eta_Q = 0.205$, $Q_{cc} = 7.2$ MHz, $\sigma_{11} = -3.51$ kHz, $\sigma_{22} = 1.83$ kHz, and $\sigma_{33} = 2.61$ kHz. Figure 4d is the simulated ^{85}Rb line shape obtained by the MC method, in which the case of noncoincident PAS frames was assumed. Note that there is not much difference between the line shapes obtained upon assumption of coincident or noncoincident PAS frames. This is because the

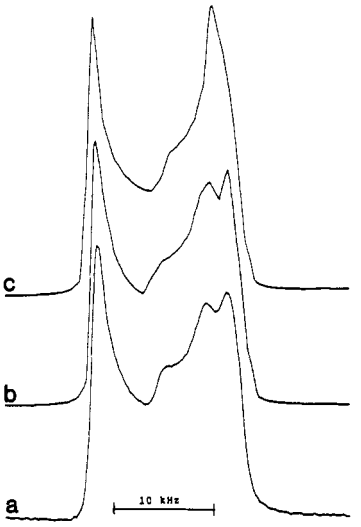

Figure 5. Comparison of the simulated and experimental ^{87}Rb powder pattern line shapes of $RbClO_4$ obtained by two different methods: (a) experimental powder pattern line shape, (b) simulated line shape assuming noncoincident PAS frames obtained by the MC method, (c) simulated line shape assuming coincident PAS frames obtained by the Baugher method.

large value of Q_{cc} for ^{85}Rb makes the chemical shielding contribution to the line shape relatively insignificant. The values of η and Q_{cc} can be used as starting guess data for the ^{87}Rb simulations. In contrast, Figure 5c is the result of a line-shape simulation for ^{87}Rb in $RbClO_4$ using the Baugher method with η_Q = 0.18, Q_{cc} = 3.4 MHz, and three principal values of −0.01, 0.20, and 0.68 kHz for the CSA tensor. This is the best result we can obtain for the condition of coincident frames, i.e. by the Baugher method. Note that the match is not very good. For example, there are three peaks in the experimental ^{87}Rb line shape in Figure 5a, but only two peaks for the simulated one in Figure 5c, and the intensities of two peaks in the simulated result do not match well with those in the experimental line shape. Figure 5b is the simulated line shape obtained by assuming noncoincident frames with σ_{11} = −0.46 kHz, σ_{22} = −0.08, σ_{00} = 2.02 kHz, η_Q = 0.16, Q_{cc} = 3.2 MHz, and Euler angles α = 58°, β = −81°, and γ = 62°, obtained by the MC method. The better match between Figure 5a and Figure 5b clearly proves the existence of noncoincident frames for ^{87}Rb in $RbClO_4$. It should also be noted that there is a considerable difference between the shielding tensor elements obtained by the Baugher method and those obtained by the MC method for noncoincident PAS frames. *This demonstrates the fact that shielding tensor elements obtained by the Baugher method do not represent the true shielding tensor elements, which can only be obtained by a method that allows for noncongruency of the PAS frames.*

From these results it seems that ^{87}Rb line shapes are much more sensitive to the existence of noncoincident PAS frames than are ^{85}Rb line shapes. As we will discuss later, the η_Q value for the quadrupole tensor for ^{85}Rb should be the same as that of ^{87}Rb and there will be better accuracy in a measurement of η_Q for ^{85}Rb from the Baugher method. From this independent calculation, the resulting η_Q value of 0.16 from the noncoincident frame is also close to the η_Q value obtained for ^{85}Rb. Another important point, when one is comparing the use of the two nuclides, is the fact that the shielding tensor elements obtained by the Baugher method for both ^{87}Rb and ^{85}Rb are very different. As the chemical environments are the same for the two nuclides, the chemical shielding tensor elements should be the same for both nuclides. The ^{87}Rb line shapes should give the more accurate shielding data, and the difference between the shielding elements obtained for the two nuclides clearly demonstrates the difficulty of extracting chemical shielding data from the broader ^{85}Rb line shapes.

In an effort to convey the level of confidence associated with the extracted NMR parameters from the simulated line shapes, we have provided Figure 6. In this figure we demonstrate the

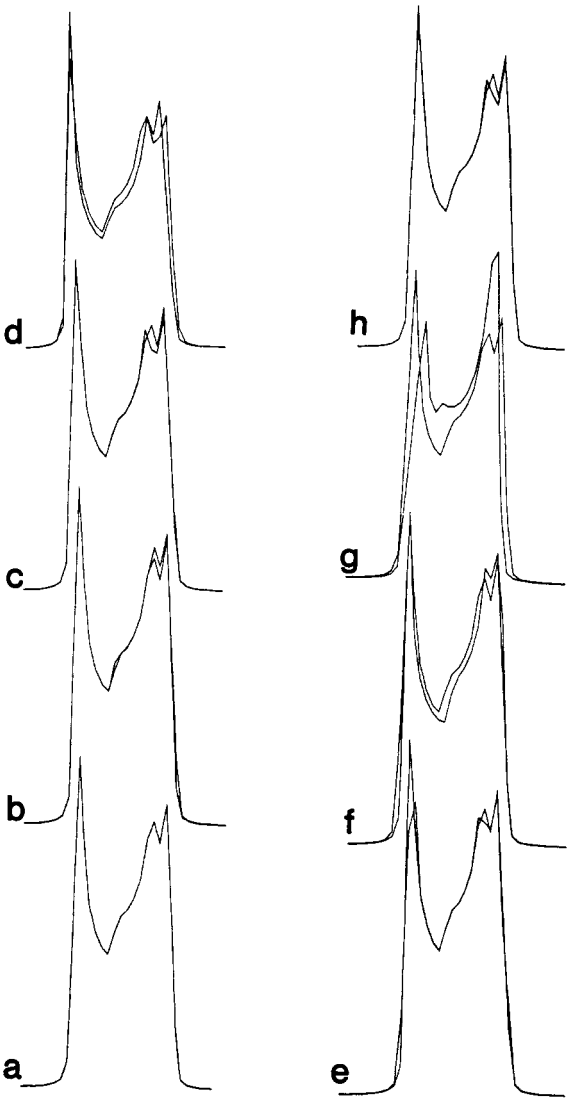

Figure 6. Superposition of the "best fit" simulated line shape of $RbClO_4$ with line shapes obtained by a small variation of η_{CS}, η_Q, Q_{cc}, α, β, and γ from their "best fit" values. In b–h, the line shape that is superimposed on the "best fit" line shape is described only in terms of the amount by which the particular parameter was varied. The normalized error is also given. Conditions: (a) "best fit" simulated line shape, error = 0.000; (b) η_{CS} varied by +0.035, error = 0.326; (c) η_Q varied by +0.035, error = 0.326; (d) Q_{cc} varied by +0.1 MHz, error = 1.250; (e) α varied by +4°, error = 3.173; (f) β varied by −1°, error = 2.271; (g) β varied by −2°, error = 14.429; (h) γ varied by +4°, error = 0.041.

sensitivity of the ^{87}Rb simulated line shape for $RbClO_4$ to small changes of the NMR parameters, η_{CS} (b), η_Q (c), Q_{cc} (d), α (e), β (f,g), and γ (h). From Figure 6 one can get some ideal of the parameters to which the line shape is most sensitive. A normalized relative error can be calculated as follows:

$$(A - B)/B$$

where A is the error between the experimental and simulated line shapes upon small variation of a particular parameter, and B is the error between the experimental and "best fit" line shape. A comparison of the relative errors obtained on variation of the different parameters shows that the line shape is more sensitive to change in the Euler angles, particularly angles α and β, than it is to change in η_Q, Q_{cc}, or η_{CS}. This fact demonstrates the importance of noncoincident frames. For the values of the normalized relative error, see Figure 6. Hence, we can conservatively estimate that all the Q_{cc} values obtained are accurate to ±0.1 MHz, the η_{CS} values to ±0.04, η_Q values to ±0.04, α and γ values to ±4°, and β values to ±1°.

The existence of noncoincident frames for ^{87}Rb in $RbClO_4$ is not a special case; with the MC technique we have found that

TABLE II: NMR Parameters Obtained from the MC Method for ^{87}Rb in Pure Salts

compd	Q_{cc}, MHz	η_Q	$\Delta\sigma$, ppm	η_{CS}	σ_0, ppm	α, deg	β, deg	γ, deg
Rb_2SO_4 (1)	2.65	0.89	−16.20	0.43	46.6	73	43	48
$RbOOCH\cdot H_2O$	2.83	0.30	26.05	1.00	0.0	58	−83	63
$RbClO_4$	3.19	0.16	17.50	0.25	3.8	58	−81	62
Rb_2CO_3 (2)	3.20	1.00	−33.62	0.26	−7.0	0	−3	11
Rb_2SO_4 (2)	3.21	0.13	13.37	0.01	3.0	18	−87	68
$RbOH\cdot H_2O$	4.32	0.77	−115.76	0.42	30.5	−21	23	48
Rb_2CO_3 (1)	5.00	0.75	27.51	0.26	18.9	57	16	16
Rb_2CrO_4 (1)	5.23	0.48	223.79	0.25	−47.4	28	−15	37
$RbAc\cdot H_2O$	6.91	0.47	−10.47	0.01	7.6	17	−13	15
Rb_2CrO_4 (2)	11.53	0.75	−19.71	0.16	52.8	0	74	−77

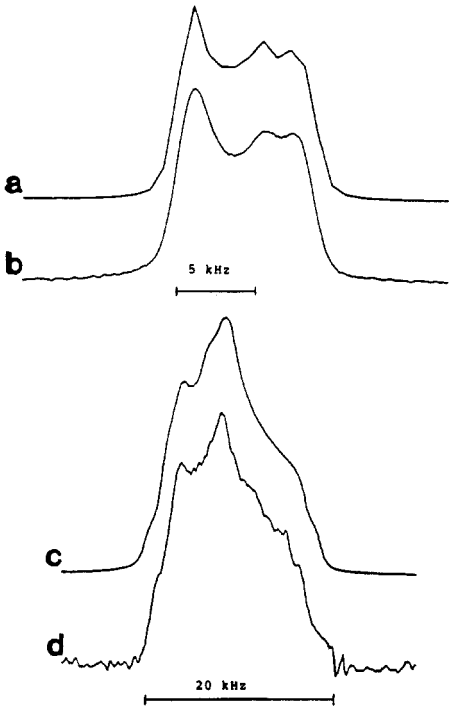

Figure 7. Comparison of the experimental and simulated central transition powder pattern line shapes of ^{87}Rb in $RbOOCH\cdot H_2O$ and $RbOH\cdot H_2O$ obtained assuming noncoincident PAS frames: (a) simulated line shape of $RbOOCH\cdot H_2O$ obtained with the MC method, (b) the experimental powder pattern of $RbOOCH\cdot H_2O$, (c) the simulated line shape of proton decoupled $RbOH\cdot H_2O$ obtained with the MC method, (d) experimental powder pattern of ^{87}Rb in $RbOH\cdot H_2O$ with proton decoupling.

several other rubidium compounds such as $RbOOCH\cdot H_2O$ and Rb_2SO_4 also show the same interesting properties. Table II lists all the NMR constants obtained by this MC method. Figure 7a,b and Figure 7c,d show how well the ^{87}Rb simulated and experimental line shapes match for $RbOOCH\cdot H_2O$ and $RbOH\cdot H_2O$, respectively. Figure 8 shows the match between the simulated and experimental ^{87}Rb line shapes of $RbOOCCH_3\cdot H_2O$. From the structure data,[11] both the Cs and Rb compounds associated with the same anion have very similar unit cell structures. For example, $RbClO_4$ has the same orthorhombic crystal structure and four equivalent sites in one unit cell as $CsClO_4$, both Cs_2SO_4 and Rb_2SO_4 have two distinct sites in the unit cell with the orthorhombic structure, and both $CsNO_3$ and $RbNO_3$ have three distinct sites in the unit cell. We expect some of the NMR

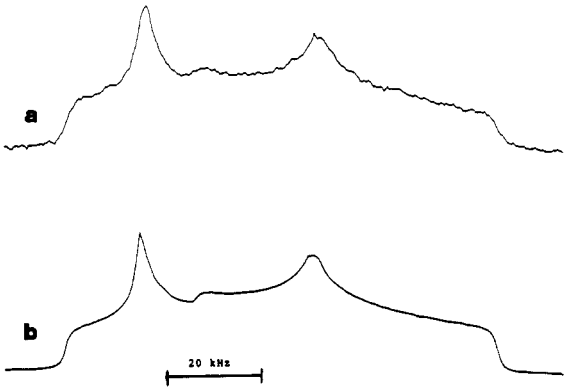

Figure 8. Comparison of the simulated and experimental ^{87}Rb powder pattern line shapes of $RbOOCCH_3\cdot H_2O$: (a) experimental powder pattern and (b) simulated line shape obtained by the MC method.

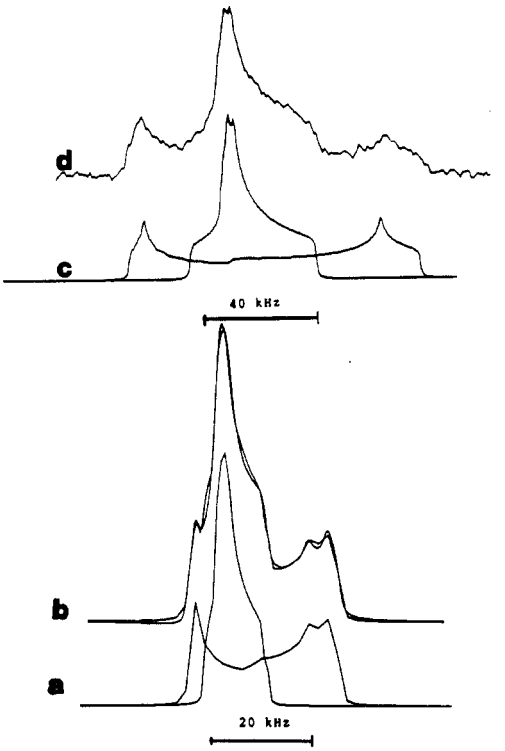

Figure 9. Overlapping components of the central transition powder pattern line shapes for ^{87}Rb and ^{85}Rb in Rb_2SO_4 and their deconvolutions: (a) deconvolution of the two contributions to the ^{87}Rb line shape obtained by the MC method, (b) superposition of the simulated and experimental ^{87}Rb line shapes, (c) ^{85}Rb experimental powder pattern of Rb_2SO_4, (d) deconvolution of the two components of c by the Baugher method.

parameters of these two nuclides to show some similarities. Mooibroak et al.[12] have reported the following data from an analysis of the NMR data on $CsClO_4$, $\eta_Q = 0.09$ and $\Delta\sigma = 36$ ppm. These values are somewhat close to the values $\eta_Q = 0.16$ and $\Delta\sigma = 17.5$ ppm for $RbClO_4$. Parts b and d of Figure 9 show the experimental powder patterns of the ^{87}Rb and ^{85}Rb nuclides, respectively, in Rb_2SO_4. The superposition of the two contributions to the ^{87}Rb line shape deconvolved by the MC method, followed by comparison with the experimental line shape, clearly shows that there are two nonequivalent nuclei in the unit cell as we have discussed. Parts a and c of Figure 9 are the deconvolutions of these two contributions in the ^{87}Rb and ^{85}Rb cases, respectively. As discussed by Mooibroak et al., two distinct sites in the unit cell of Cs_2SO_4 cannot be easily observed from the powder pattern

(11) $RbClO_4$, $CsClO_4$: Braeken, H.; Harang, L. *Z. Krist.* **1930**, *75*, 538. $CsNO_3$: Segel, S. L. *J. Chem. Phys.* **1980**, *73*, 4146. $RbNO_3$: Dean, C.; Hambley, T. W.; Snow, M. R. *Acta Crystallogr.* **1984**, *C40*, 1512. Rb_2SO_4: Nord, A. G. *Acta Crystallogr.* **1974**, *B30*, 1640. Cs_2SO_4: Fischmister, H. F. *Monatch. Chem.* **1962**, *93*, 420. RbF: Weir, P. *J. Chem. Phys.* **1964**, *37*, 1887. RbCl: Deshpande, V. T.; Sirdeshmukh, D. B. *Acta Crystallogr.* **1961**, *14*, 353. RbBr: Swanson, H. E., et al. *Natl. Bur. Stand. Circ. (U.S.)* **1957**, *539*, 7, 43. RbI: Sirdeshmukh, D. B.; Deshpande, V. T. *Curr. Sci.* **1964**, *33*, 428.

(12) Mooibroak, S.; Wasylishen, R. E.; Dickson, R.; Facey, G. *J. Magn. Res.* **1986**, *66*, 542.

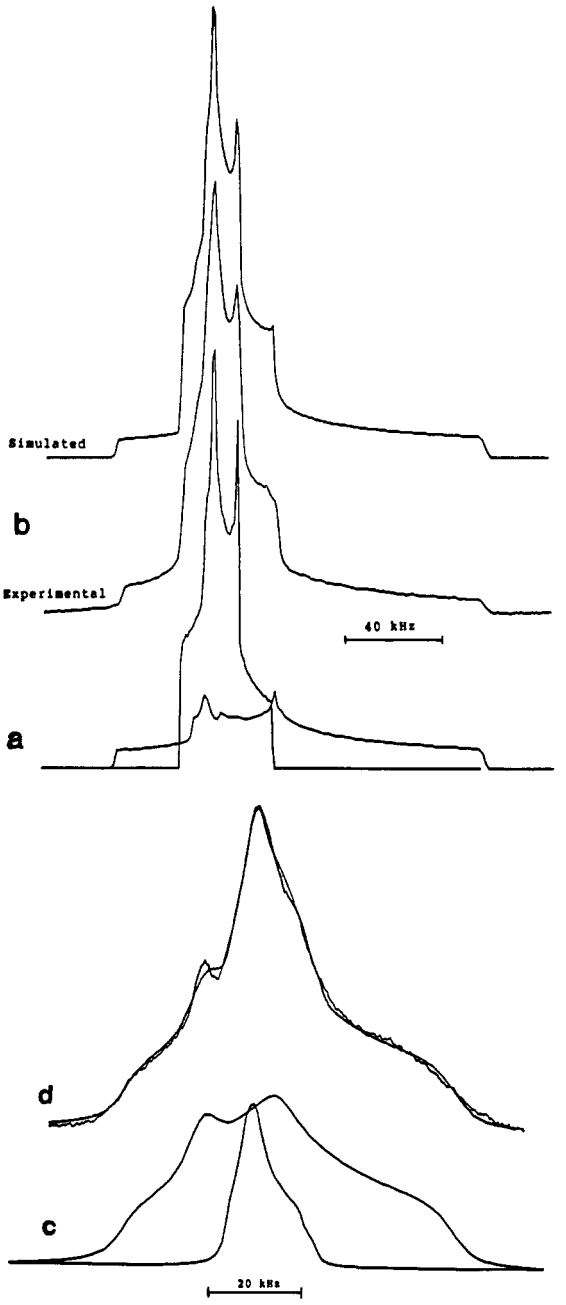

Figure 10. Overlapping components of the central transition powder pattern line shape for ^{87}Rb in Rb_2CrO_4 and Rb_2CO_3 and their deconvolutions: (a) deconvolution of the two components of the line shape of Rb_2CrO_4 obtained by the MC method, (b) comparison of the simulated and experimental powder pattern line shapes of Rb_2CrO_4, (c) deconvolution of the two components of the line shape of Rb_2CO_3 obtained by the MC method, (d) comparison of the simulated and experimental line shapes of Rb_2CO_3.

unless the magic angle spinning (MAS) technique is applied. It is quite interesting that both Cs and Rb nuclei have the same type of structure in the unit cell, and yet have significant differences in their quadrupolar coupling constants. With Rb_2SO_4 taken as an example, the larger quadrupolar moment makes the rubidium compound more sensitive than the cesium compound in distinguishing a structural difference from the quadrupole powder pattern, whereas the cesium compound is more sensitive to distinct site differences via the shielding tensor. In the same vein, parts a and c of Figure 10 show the deconvolution of the two components of the Rb_2CrO_4 and Rb_2CO_3 line shapes, respectively, while parts b and d show the comparison of the simulated and experimental line shapes of Rb_2CrO_4 and Rb_2CO_3.

$RbClO_4$ and Rb_2SO_4, which were discussed above, are typical examples of rubidium compounds with different numbers of Rb

TABLE III: Structure of Rubidium Salts and the Distinct Sites in the Unit Cell

compd	structure	site	ref
$RbClO_4$	orthorhombic	1	12
$RbOH·H_2O$	orthorhombic	1	12
$RbOOCCH_3·H_2O$		1	*a*
$RbOOCH·H_2O$		1	*a*
Rb_2CrO_4	orthorhombic	2	12
Rb_2CO_3	monoclinic	2	12
Rb_2SO_4	orthorhombic	2	12
$RbNO_3$	trigonal	3	12
RbF	cubic	1	12
RbCl	cubic	1	12
RbBr	cubic	1	12
RbI	cubic	1	12

[a] Our work.

TABLE IV: NMR Quadrupole Parameters for ^{85}Rb in Pure Salts

compd	η_Q	Q_{cc}, MHz	σ_0, ppm	Q_{cc}/Q, MHz/10^{-24} cm^2
RbF	0	0	59	
RbCl	0	0	123	
RbBr	0	0	148	
RbI	0	0	181	
$RbOH·H_2O$	0.72	5.09	51	25
$RbOOCH·H_2O$	0.30	5.20	3	19
Rb_2SO_4 (1)	0.93	5.48	*a*	20
Rb_2CrO_4 (1)	0.40	7.00	*a*	26
$RbClO_4$	0.20	7.20	*b*	27
Rb_2CO_3 (2)	1.00	10.00	*a*	37
Rb_2SO_4 (2)	0.12	10.75	*a*	39
Rb_2CO_3 (1)	0.60	14.50	*a*	53
Rb_2CrO_4 (2)	*b*	*b*	*b*	
$RbAc·H_2O$	*b*	*b*	*b*	
$RbNO_3$	*c*	*c*		

[a] Data is not accurate due to large Q_{cc}. [b] Line shape is too distorted to extract data. [c] Cannot resolve the overlapped tensors.

TABLE V: NMR Quadrupole Parameters for ^{87}Rb in Pure Salts

compd	η_Q	Q_{cc}, MHz	σ_0, ppm	Q_{cc}/Q, MHz/10^{24} cm^2
RbF	0	0	58	
RbCl	0	0	128	
RbBr	0	0	155	
RbI	0	0	183	
Rb_2SO_4 (1)	0.89	2.6	46.6	20.0
$RbOOCH·H_2O$	0.30	2.8	0.0	21.7
$RbClO_4$	0.16	3.2	3.8	24.5
Rb_2CO_3 (2)	1.00	3.2	−7.0	24.6
Rb_2SO_4 (2)	0.13	3.2	3.0	24.6
$RbOH·H_2O$	0.77	4.3	30.5	33.2
Rb_2CO_3 (1)	0.75	5.0	18.9	38.5
Rb_2CrO_4 (1)	0.48	5.2	−47.4	40.0
$RbAc·H_2O$	0.47	6.9	7.6	53.1
Rb_2CrO_4 (2)	0.75	11.5	52.8	88.5
$RbNO_3$	*a*	*a*	*a*	

[a] Cannot resolve the overlapped line shape.

sites. Table III lists the number of distinct sites in the unit cell and the structure types for some rubidium compounds. RbOH, RbOOCH, $RbOOCCH_3$, and $RbClO_4$ all show one Rb site, while Rb_2SO_4, Rb_2CrO_4, and Rb_2CO_3 have two distinct sites in their unit cell. $RbNO_3$ shows three distinct sites in a small frequency range.

C. Quadrupole and Anisotropic Chemical Shielding Tensor Elements. Tables IV and V list the values of Q_{cc}, the isotropic chemical shift, the asymmetry of EFG (η_Q), and Q_{cc}/Q (where Q is the quadrupole moment) for ^{85}Rb and ^{87}Rb nuclei in a variety of pure salts. These data were obtained from exhaustive efforts to match simulated line shapes with the experimental powder patterns using the IGCP program discussed in the previous section. In all but a few cases the data for the ^{85}Rb NMR parameters is calculated on the assumption that there is only a quadrupolar

interaction for the ^{85}Rb nucleus, as a small chemical shift contribution on the order of a few kilohertz is almost indistinguishable due to the large value of Q_{cc}. All the data for the ^{87}Rb NMR parameters is calculated on the assumption that the PAS frame shielding and quadrupole tensors are noncoincident. It should be noted that when the chemical shift parameters are small relative to the quadrupole effects, (so small that they are not manifested in the line shape), the inherent accuracy of this method decreases, and the confidence level drops accordingly.

All the rubidium halides show a narrow resonance of only a few kilohertz wide. Although the quadrupole moments of ^{87}Rb and ^{85}Rb, (0.13 and 0.27) $\times 10^{-24}$ cm^2, are relatively large compared to those of some other nuclides such as ^{133}Cs or ^{23}Na, the measurable Q_{cc} from the NMR technique is proportional to the product of the quadrupole moment Q and the EFG, which is structure dependent. The cubic cell structure of rubidium halides[11] gives rise to a totally symmetrical electric field at the rubidium nuclei and causes the EFG to vanish or be very small. Hence the result of a small Q_{cc} is a relatively unbroadened central transition.

Since ^{87}Rb and ^{85}Rb nuclides have identical chemical environments in each compound, their properties such as chemical shift, η_Q, and EFG would be expected to be identical. The η_Q and EFG (equal to Q_{cc}/Q) values of $^{85}RbClO_4$ are 0.20 and 27 MHz/10^{-24} cm^2, respectively, which are similar to the values of 0.16 and 24.5 MHz/10^{-24} cm^2 obtained for $^{87}RbClO_4$. In fact, as shown in Tables IV and V, other salts also have the same properties as $RbClO_4$ within a small error. As in the case for the η_Q and EFG, ^{87}Rb and ^{85}Rb also have the same chemical shift for the same compound. The chemical shifts of RbI, RbBr, RbCl, and RbF for ^{87}Rb are 58, 128, 155, and 183 ppm, which are very close (within a few ppm error) to those for ^{85}Rb, which are 59, 123, 148, and 181 ppm, respectively. The chemical shifts of $RbOH\cdot H_2O$ and $RbOOCH\cdot H_2O$ are 30.5 and 0.0 ppm, respectively, for ^{87}Rb and 51 and 3 ppm for ^{85}Rb. The slightly different values are probably due to some error introduced in extracting the chemical shift from a broader line shape.

These interesting properties of twin nuclides are very useful as a probe for NMR study. From eq 3 in the Theory section, the width of the line shape is dominated by the quadrupolar interaction. For ^{85}Rb it is calculated to be about 2 times that of ^{87}Rb, while the size of CSA for ^{87}Rb is 3.4 (130.88 MHz/38.64 MHz) times that of ^{85}Rb. Hence, the ^{85}Rb nucleus can provide the most accurate information about the quadrupole iteration while the ^{87}Rb nucleus provides the more accurate CSA information.

The study of chemical shifts of very high concentration alkali-metal solutions has been reviewed by Lindman.[7] From the observation of the qualitative effects of various anions associated with the alkali-metal ion on the chemical shielding, except Li^+, it seems that there is the same effect on the chemical shifts of the alkali-metal ions Na^+, Rb^+, and Cs^+. The trend of the anion's effect on the shielding for the resonance of alkali-metal nucleus is

$$I^- < Br^- < Cl^- < CO_3^{2-} < SO_4^{2-} < H_2O < NO_3^-$$

From the measurement of the chemical shift of ^{87}Rb shown in Table V, the shielding sequence of anions associated with ^{87}Rb's chemical shift in the solid-state NMR experiment agrees quite well with that of the high-concentration solution. The solid-state shielding order is

$$I^- < Br^- < Cl^- < F^- < OH^- < OOCCH_3^- < ClO_4^- < OOCH^-$$

Compounds of CO_3^{2-}, SO_4^{2-}, and CrO_4^{2-} show only one resonance in concentrated solution, while in the solid phase these compounds show two distinct sites for ^{87}Rb nuclei in the solid-state NMR study. In order to compare the chemical shift data of these two-site compounds with that of the one-site compounds, we will assume that the isotropic chemical shift of the two-site compounds is simply the average of the isotropic chemical shifts calculated for each of the two sites. With this in mind, the average values of the chemical shift of ^{87}Rb associated with SO_4^{2-} is 24.8 ppm, with CrO_4^{2-} is 2.7 ppm, and with CO_3^{2-} is 6.0 ppm. These values are added to the shielding order, the result is as follows:

$$I^- < Br^- < Cl^- < F^- < OH^- < SO_4^{2-} < OOCCH_3^- < CO_3^{2-} < ClO_4^- < CrO_4^{2-} < OOCH^-$$

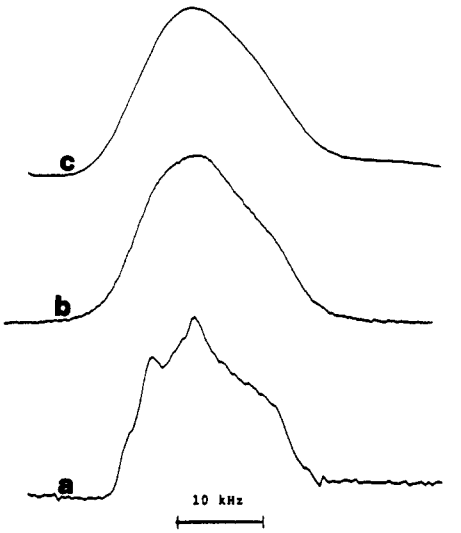

Figure 11. Dipolar interaction between protons and ^{87}Rb in $RbOH\cdot H_2O$: (a,b) powder pattern line shapes of the central transition of ^{87}Rb with, and without, decoupling, (c) convolution of part a with a 3-kHz-wide Gaussian line shape.

D. Dipolar Interaction with Protons. Parts a and b of Figure 11 show the ^{87}Rb central transition powder patterns of $RbOH\cdot H_2O$ with and without proton decoupling. The featureless line shape, obtained without proton decoupling compared to the decoupled one, clearly shows that a strong dipolar interaction exists between ^{87}Rb nuclei and protons. The structure of $RbOH\cdot H_2O$ has been reported as orthorhombic[11] $Cmc2_1$, and the dimensions of the unit cell are a = 4.12 Å, b = 11.244 Å, and c = 6.08 Å. In this structure, each rubidium nucleus is surrounded by 16 neighboring protons, eight of which belong to hydroxide and eight to water. The distances are not all equal between each proton and rubidium nucleus. The distance is 3.0–3.4 Å for protons in water and 3.4–3.8 Å for protons in hydroxide. The direct dipolar coupling interaction between a proton and rubidium nuclide is given by

$$\Delta = (\gamma_H \gamma_{Rb} \hbar^2 / r^3)(1 - 3\cos^2\theta)$$

where θ is the angle between the bond and the magnetic field $\mathbf{H}_0$. Taking the $\gamma_{1H} = 2.675 \times 10^4$ rad S^{-1} G^{-1}, $\gamma_{Rb\text{-}87} = 0.876 \times 10^4$ rad S^{-1} G^{-1}, and r = 3.2 Å, the range of dipolar splitting for a single proton would be between 1.18 and 2.36 kHz. The overall dipolar broadening effect on the Rb nucleus by these protons is dependent upon the orientation of the Rb nucleus relative to the magnetic field $\mathbf{H}_0$. Hence, the line-width contribution due to dipolar splitting for each resonance corresponding to a specific orientation will not be the same. Figure 11c is the result of convolution between a Gaussian line shape (width 3.0 kHz) and the decoupled spectra, which shows a reasonable match to the nondecoupled spectrum. Hence, we can assume the average line broading of ^{87}Rb due to nearby protons is about 3 kHz. The ^{85}Rb line shape of $Rb(H_2O)OH$ (figure not shown) displayed a smaller dipolar interaction than that of ^{87}Rb. Taking 0.23 for $\gamma_{Rb\text{-}85}$, the average broadening effect for the line shape of $RbOH\cdot H_2O$ from dipolar interaction would be only $3.0 \times 0.23/0.876 = 0.9$ kHz, which is less detectable in a very broad line shape.

Conclusions

We have combined the use of ^{87}Rb and ^{85}Rb solid-state NMR in order to demonstrate that the assumption of coincident PAS frames will lead to simulated line shapes that are dissatisfactory when compared with experimental line shapes. We have developed our own IGCF program in order to simulate the ^{87}Rb line shapes obtained for a number of simple salts, assuming noncoincident

PAS frames. The significantly different values of the Q_{cc}'s of the two nuclei can be used to our advantage in that ^{85}Rb, with its larger quadrupole moment, can give us an indication of the number of chemically different rubidium atoms in the salts. It also provides a good starting guess data set, obtained by the Baugher method, for our ^{87}Rb simulations. The ^{87}Rb nuclei, with their smaller quadrupole moment, provide us with line shapes that are sensitive to the consequences of noncoincident PAS frames. The fact that the shielding tensor elements obtained by the Baugher and MC methods are so different clearly demonstrates the importance of assuming noncoincidence of the PAS frame when one wishes to extract the correct shielding tensor elements from a powder line shape. We believe that other nuclei with relatively small quadrupole moments, e.g. ^{133}Cs, can benefit from the inclusion of noncoincident PAS frames in powder line-shape calculations, in order to obtain satisfactory correlation between simulated and experimental line shapes.

Acknowledgment. We express our appreciation to the NSF for partial support of this work via awards CHE 85-44272 and CHE 86-13421. Further, we acknowledge partial support from the College of Science and Mathematics at the University of South Carolina for partial support of J. T. Cheng.

Registry No. $RbClO_4$, 13510-42-4; RbOH, 1310-82-3; Rb_2CrO_4, 13446-73-6; $RbOOCH \cdot H_2O$, 123676-89-1; $RbOOCCH_3 \cdot H_2O$, 123676-90-4; Rb_2SO_4, 7488-54-2; Rb_2CO_3, 584-09-8; $RbNO_3$, 13126-12-0; RbF, 13446-74-7; RbCl, 7791-11-9; RbBr, 7789-39-1; RbI, 7790-29-6; ^{85}Rb, 13982-12-2; ^{87}Rb, 13982-13-3.

Aggregation in Five-Coordinate High-Spin Natural Hemins: Determination of Solution Structure by ^1H NMR

Shyamalava Mazumdar and Samaresh Mitra*

Chemical Physics Group, Tata Institute of Fundamental Research, Homi Bhabha Road, Bombay 400 005, India *(Received: April 4, 1989; In Final Form: June 9, 1989)*

^1H NMR measurements (at 500 MHz) of nuclear spin–spin relaxation time T_2 (from NMR line width) at different temperatures are reported for aggregates of several five-coordinate high-spin iron(III) complexes of proto-, deutero-, and coproporphyrins in solution and are utilized to determine their solution structure. Extensive aggregation of these complexes in solution is observed, and the dominant form of the aggregates is shown to be dimers. The degree of aggregation for these iron(III) porphyrins follows the order proto- $\gg$ deutero- $>$ copro-. The line width of the heme methyl resonances was analyzed by using a nonlinear least-squares fit program working in finite difference algorithm. The values of T_2 were used to determine the structural details of the dimer.

Introduction

Porphyrins and metalloporphyrins, like many other aromatic π-electron systems, show significant tendency to form aggregates in solutions.[1,2] The π–π interaction of aromatic donor or acceptor molecules with porphyrins and metalloporphyrins has been studied by different techniques.[3-12] It has been proposed that in some of the redox hemoproteins, e.g., cytochrome c_3, the π interaction between the heme groups and the phenylalanine moiety plays an important role in decreasing the redox potential of these systems.[13,14] Heme–heme interaction is also known to play an important role in the structure of photosynthetic pigments.[15]

Proton NMR has been extensively used for the study of the aggregation of porphyrins and metalloporphyrins in solution.[16-23] LaMar et al.[17-23] have reported extensive NMR studies on aggregation of metalloporphyrins and have shown that nuclear magnetic relaxation measurements can be successfully used to elucidate the structure of aggregates in solution. They have reported measurements of nuclear spin–lattice relaxation time (T_1) as a function of concentration for low-spin bis cyano complexes of 2,4-dibromodeuterohemin in methanol and of protohemin in aqueous alkali-metal solutions.[17-21] These studies have shown that the nature of the aggregate and its structure depend on the solvent as well as on the nature of the substituents in the porphyrin ring. The solution structure for the aggregates of these six-coordinate low-spin hemins deduced by LaMar et al.[17-21] consisted of slipover type dimers formed by π stacking between one or two pyrrole rings of two hemin bis cyanide monomers. Similar studies on five-coordinate high-spin hemins (Figure 1) are however very limited because the line widths of these high-spin hemin proton resonances are generally larger compared to the low-spin complexes. The

(1) (a) Scheer, H.; Katz, J. J. In *Porphyrins and Metalloporphyrins*; Smith, K. M., Ed.; Elsevier: Amsterdam, 1975; p 398. (b) Brown, S. B.; Jones, P. *Biochem. J.* **1970**, *117*, 733.
(2) White, W. I. In *The Porphyrins*; Dolphin, D., Ed.; Academic: New York, 1978; Vol. V, p 303.
(3) Selnut, J. A. *J. Phys. Chem.* **1984**, *88*, 4988.
(4) Boyd, P. D. W.; Smith, T. D. *J. Chem. Phys.* **1972**, *56*, 1253.
(5) Blumberg, W. E.; Peisach, J. *J. Biol. Chem.* **1965**, *240*, 870.
(6) Hofstra, U.; Koehorst, R. B. M.; Schaafsma, T. *Magn. Reson. Chem.* **1987**, *25*, 1069.
(7) Pasternach, R. F.; Huber, P. R.; Boyd, P.; Engasser, G.; Francesconi, L.; Gibbs, E.; Fasella, P.; Venturo, G. C. *J. Am. Chem. Soc.* **1972**, *94*, 4511.
(8) Fulton, G. P.; LaMar, G. N. *J. Am. Chem. Soc.* **1976**, *98*, 2124.
(9) (a) Fulton, G. P.; LaMar, G. N. *J. Am. Chem. Soc.* **1976**, *98*, 2119. (b) Kabbani, A. T.; LaMar, G. N. *J. Magn. Reson.* **1981**, *43*, 90.
(10) Doughty, D. A.; Dwiggins, C. W., Jr. *J. Phys. Chem.* **1969**, *73*, 423.
(11) Boas, J. F.; Pilbrow, J. R.; Smith, T. D. *J. Chem. Soc. A* **1969**, 721.
(12) Shelnut, J. A. *J. Phys. Chem.* **1984**, *88*, 4988.
(13) Antonini, E.; Brunori, M. In *Hemoglobins and Myoglobins in Their Reactions with Ligands*; North-Holland: Amsterdam, 1971; Chapter 4.
(14) (a) Inokuchi, H. In *Biomimetic Chemistry*; Yoshida, Z., Norie, I., Ed.; Kodansha Ltd.: Tokyo, 1983; p 101. (b) Haser, R.; Pierrot, M.; Frey, M.; Payan, F.; Astier, J. P.; Bruschi, M.; Gall, J. L. *Nature* **1979**, *282*, 806.
(15) (a) Boxer, S. G. *Biochim. Biophys. Acta* **1985**, *726*, 265. (b) Katz, J. J.; Dougherty, R. C.; Boucher, L. J. In *The Chlorophylls*; Verman, L. P., Seely, G. R., Ed.; Academic: New York, 1966; p 185.
(16) Goff, H. M. In *Iron Porphyrins*; Lever, A. B. P., Gray, H. B., Eds.; Addison-Wesley: Reading, MA, 1983; Part 1, Chapter 4, p 239.
(17) LaMar, G. N.; Walker, F. A. In *The Porphyrins*; Dolphin, D., Ed.; Academic: New York, 1979; Vol. IV, p 61.
(18) Viscio, D. B.; LaMar, G. N. *J. Am. Chem. Soc.* **1978**, *100*, 8092.
(19) Viscio, D. B.; LaMar, G. N. *J. Am. Chem. Soc.* **1978**, *100*, 8096.
(20) LaMar, G. N.; Minch, M. J.; Frye, J. S. *J. Am. Chem. Soc.* **1981**, *103*, 5383.
(21) LaMar, G. N.; Visco, D. B. *J. Am. Chem. Soc.* **1974**, *96*, 7354.
(22) Snyder, R. V.; LaMar, G. N. *J. Am. Chem. Soc.* **1977**, *99*, 7178.
(23) Migita, K.; LaMar, G. N. *J. Phys. Chem.* **1980**, *84*, 2953.

0022-3654/90/2094-0561$02.50/0